A photo rechargeable capacitor based on the p–n heterojunction of ZnO/ZIF-67 showing enhanced photovoltage ⊕

Yanlong Lv; Xin Sun; Changhua Mi; Jianan Gu ⊕ ; Yanhong Wang; Meicheng Li ✉ ⊕

Check for updates

View Online   Export Citation

Articles You May Be Interested In

Hydrogeological modeling of the groundwater recharge feeding the Chambo aquifer, Ecuador

AIP Conf. Proc. (November 2018)

The use of sand column in recharge reservoir to reduce sea water intrusion

AIP Conf. Proc. (October 2020)

Synthesis of different manganese dioxide nanostructures and studding the enhancement of their electrochemical behavior in zinc – Mno_2 rechargeable batteries by doping with copper

AIP Conf. Proc. (March 2020)

A photo rechargeable capacitor based on the p–n heterojunction of ZnO/ZIF-67 showing enhanced photovoltage ⓔⓟ

View Online   Export Citation   CrossMark

Yanlong Lv, Xin Sun, Changhua Mi, Jianan Gu, ⓘ� Yanhong Wang, and Meicheng Li[a] ⓘ

AFFILIATIONS

State Key Laboratory of Alternate Electrical Power System with Renewable Energy Sources, School of New Energy,
North China Electric Power University, 100096 Beijing, China

[a]Author to whom correspondence should be addressed: mcli@ncepu.edu.cn

ABSTRACT

The photo rechargeable device (PRD) has been continuously drawing attention because it combines energy conversion and storage in one device. As for the photoelectrode of PRD, the construction of heterojunction is of crucial importance to enhance the photo performance. In this work, a two-electrode photo rechargeable capacitor based on the p–n heterojunction of ZnO/ZIF-67 is fabricated. ZIF-67 not only serves as the energy storage material but also forms the p–n heterojunction together with ZnO. A fast volatilization method was adopted for the *in situ* growth of ZIF-67 on ZnO nanorods to ensure sufficient mass loading and fewer interface defects. The results show a photovoltage of 0.36 V (0.2 V higher than single ZnO), a specific capacitance of 759.0 mF/g, and an overall energy conversion efficiency of 0.49%. The enhanced photovoltage is attributed to the p–n heterojunction. Moreover, a practical button cell was also fabricated, with 91% Coulombic efficiency remaining after 3000 cycles in the dark.

I. INTRODUCTION

At the present time, the full utilization of renewable energy is highly demanded because of the growing worldwide concerns about the risk of traditional fossil fuels.[1,2] Solar energy, with its availability and lower cost, can provide an abundant source of renewable energy.[3–5] However, solar energy has to be stored because of its unstable nature.[6,7] Photo rechargeable devices (PRDs), combining the photovoltaic (PV) part and energy storage (ES) part in a single device, could make full use of solar energy and solve the storage problem at the same time.[8–12]

The idea of the integration of PV and ES devices was applied years ago. Photo rechargeable batteries and photo rechargeable capacitors (PCs) are two common PRDs.[8,13–18] Compared with batteries, capacitors have a rapid response to current changes and a long lifetime of redox-free electrolytes. The first photo capacitor was reported by Tsutomu Miyasaka in 2004.[19] Since then, a number of PCs have been developed, such as the photo dye-sensitized solar cell,[20,21] organic semiconductor solar cell,[22] and perovskite solar

cell[23] combining the capacitors. On the other hand, the PRDs can be separated into two categories based on the number of electrodes: two electrodes and three electrodes. There will be a working electrode attached to the PV and a counter electrode in a two-electrode device, while an additional electrode exists as a bridge between the PV and ES parts in the three-electrode device. The two-electrode device has advantages in the cost, volume, and weight of the electrode material. However, the simplified structure of the two-electrode makes it hard to make use of the above mentioned types of PV materials, leading to an efficiency drop compared with the three-electrode. So the challenge is how to achieve as good a photo performance as possible while keeping the simplified structure.

The construction of heterojunction, especially p–n heterojunction, is one of the most commonly used strategies to enhance photo performance. The internal electric field in the p–n heterojunction could induce charge separation with additional driving force and generate energy band bending to enhance photo activity.[24] Another benefit is that the band gaps of the heterojunction can be controlled by coupling different gap energy levels to achieve better visible-light

09 February 2025 02:37:53

adsorption. Kumar and co-workers build a type II heterojunction of MoS_2 and MoO_x for photo rechargeable Li-ion batteries.[25] The staggered energy band alignment of MoS_2 and MoO_x limits electron–hole recombination. Yu and co-workers employed the heterojunction of TiO_2 and Fe_2O_3 to regulate the electronic structure of TiO_2 for Li–O_2 batteries, which show an ultra low overpotential of 0.19 V.[26] Particularly in the two-electrode structure of PRD, materials with bifunctional uses are favored. For example, Volder and co-workers prepared a photocathode of ZnO and MoS_2 for Zn-ion batteries. MoS_2 is not only important for solar energy conversion because of its lower bandgap, but it can also store zinc ions.

Since the heterojunction is crucial for the photo performance of PRDs, the composition should be carefully chosen. Herein, we report a two-electrode PC based on ZnO/ZIF-67. The ZnO/ZIF-67 heterojunction was adopted for several reasons. First, ZnO and ZIF-67 are potential candidates for PV and ES, respectively. ZnO is a photo active material with a wide bandgap, outstanding electron mobility, and considerable exciton binding energy.[27–30] ZIF-67, one of the most representative metal–organic frameworks (MOFs), has a high surface area, adjustable pore sizes, and open metal sites, making it suitable as a capacitor material.[31,32] Second, the semiconductor behavior of MOF has been studied since 2007.[33] ZIF-67 is a p-type material; the combination of ZnO and ZIF-67 can build a p–n heterojunction. Third, the two materials have good compatibility. A fast volatilization method was used to *in situ* grow ZIF-67 onto ZnO nanorods, which could avoid obvious voids and reduce interface defects. Meanwhile, the ZIF-67 shell can protect ZnO from corrosion from the electrolyte.[34] As a result, the ZnO/ZIF-67 PCs show a photovoltage of ~0.36 V under 1 sun illumination and a capacitance of 759.0 mF/g in a neutral solution of 0.5M Na_2SO_4. A button cell was also fabricated to test its practical use. The Coulombic efficiency remained at 91% after 3000 cycles in the dark.

II. MATERIALS AND METHODS

A. Materials

Zinc nitrate hexahydrate ($Zn(NO_3)_2·6H_2O$, 98%, Acros), hexamethylenetetramine ($C_6H_{12}N_4$, 99.5%, Acros), cobalt nitrate hexahydrate ($Co(NO_3)_2·6H_2O$, 98%, Sigma-Aldrich), 2-methylimidazole ($C_4H_6N_2$, 99%, Acros), and methanol (CH_4O, 99.8%, Sigma-Aldrich) were used.

B. Synthesis of ZnO/ZIF-67 heterojunction

The ZnO nanorods were synthesized through a typical hydrothermal process. The ITO glasses were cut into $1.5 × 1.0$ cm^2 pieces and sonicated in water, ethanol, and acetone for 30 min. ZnO nanoseeds were precoated onto the ITO surface. The ZnO nanoseeds were prepared in a 10 ml ethanol solution of 15 mg zinc acetate dihydrate with a stirring time of 10 h. The solution was dropped onto the ITO glass with a rotation rate of 3000 r/min. The dropping process was repeated for another round. Then the ITO glass was heated for 1 h at 150 °C. Finally, the ITO was put into a solution of 1.5 g zinc nitrate hexahydrate, 0.75 g hexamethylenetetramine, and 75 ml water. The solution was heated in a hydrothermal kettle at 95 °C for 11 h. The ITO glass was then washed in water and dried in the air. A white membrane was observed on the surface of the ITO glass.

The *in situ* growth of ZIF-67 onto the ZnO nanorods was executed at room temperature. The ITO glass with ZnO nanorods was put into a solution of 1.5 g 2-methylimidazole (2-IM), 0.75 g cobalt nitrate hexahydrate, and 50 ml methanol. The solution was kept at 55 °C for 15 h. After washing and drying at room temperature, the final product was a purple membrane on the surface of the ITO glass.

C. Fabrication of PSc cell

The PSc cell was assembled using a 2045-type optical coin cell model. The as-prepared ZnO/ZIF-67 ITO glasses (12 mm in diameter) were used as the cathode. ZIF-67 was deposited on the Ni foam (12 mm in diameter) and used as the anode. The separator membrane was a Whatman glass microfiber filter paper separator (16 mm in diameter) with the addition of 150 μl of 0.5M Na_2SO_4 aqueous electrolyte. Moreover, an 8 mm-diameter hole was designed as an optical window in the center of the cathode case. The ITO glass was fixed using silica gel before assembling the optical cell.

D. Physiochemical characterization and electrochemical measurements

X-ray diffraction (Rigaku SmartLab SE) was performed to characterize the crystal structures. SEM (ZEISS Gemini SEM 300) was employed to investigate the morphologies of the samples. X-ray photo-electron spectroscopy (XPS, Thermo Scientific K-Alpha) was used to describe the elemental composition of the samples. Photoelectrochemical (PEC) measurements were done in a photo electrochemical cell with an CHI 760E electrochemical workstation. A Ni foam coated ZIF-67 was used as the counter electrode, and an Ag/AgCl electrode was used as the reference electrode. The electro performance was characterized under simulated sunlight illumination at 100 mW cm^{-2} (300 W xenon lamp, AM 1.5 G filter). Electrochemical impedance spectroscopy (EIS) curves were obtained at frequencies ranging from 100 kHz to 0.1 Hz under the open circuit potential. The cyclic voltammetry (CV) measurements were performed from −0.5 to 0.5 V at scan rates from 0.01 to 0.5 V/s. The Mott–Schottky curves were collected at a frequency of 1 kHz under the dark condition. Na_2SO_4 solution (0.5M) was used as the electrolyte for all the PEC measurements in our experiments.

III. RESULTS AND DISCUSSIONS

A simple schematic illustration of the photocharging mechanism is shown in Fig. 1. The photocathodes of ZnO/ZIF-67 are designed to yield the photocharging effect (see further). The synthesis procedure for ZnO/ZIF-67 PCs was shown in the experiment method part. The SEM was done to view the morphology of ZnO/ZIF-67. The surface and cross section images of ZnO are shown in Figs. 2(a) and 2(b), respectively. The ZnO nanorods show an ordered rod-like hexagonal morphology with a diameter of ~200 nm and a length of ~3 μm. Several particles with a size less than 200 nm were observed in Fig. 2(c). A fast volatilization method was used to fabricate ZIF-67 onto the surface of ZnO. During the preparation process, methanol was chosen as the solvent because of its volatility. The methanol volatilization was utilized to accelerate the precipitation at the interface of the solution. Consequently, the
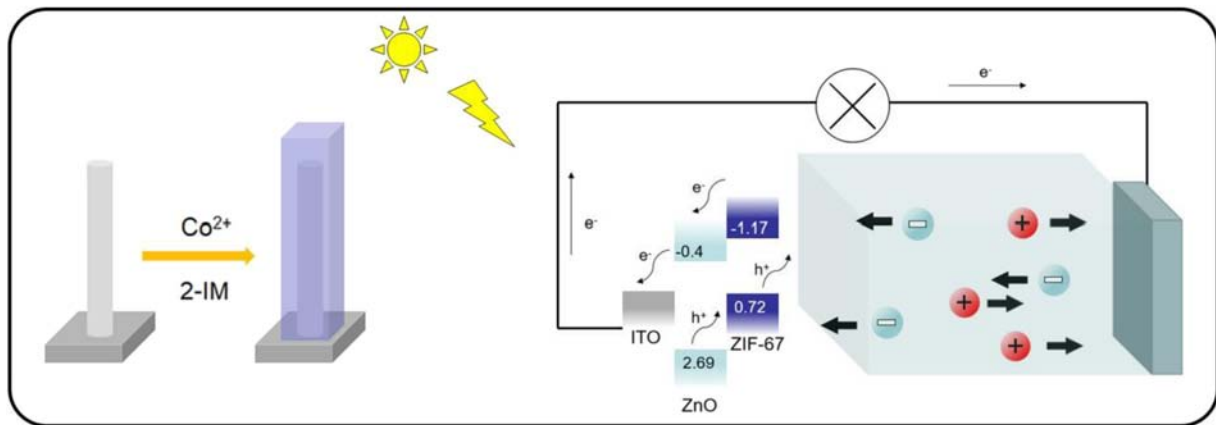
FIG. 1. Schematic illustration of the proposed photocharging mechanism of ZnO/ZIF-67 PCs.

ZIF-67 with small sizes was formed because of the shortened crystallization time. As shown in the cross section image in Fig. 2(d), it can be observed that the ZIF-67 successfully fills the voids of the ZnO nanorods, suggesting a good contact between ZnO and ZIF-67. This is perhaps because, during the synthesis process, the surface Zn atoms of ZnO could be dissolved to be Zn ions because of the weak alkalinity of 2-IM. Afterward, the Zn ions and Co ions in the solvent will react with 2-IM to form MOFs on the surface of ZnO. In the heterojunction, fewer voids mean fewer interface defects, which will help reduce the charge transfer resistance. To further confirm the heterojunction of ZnO/ZIF-67, we have done the TEM mapping of ZnO/ZIF-67 (Fig. S1). As can be observed, the distribution of elements Zn, Co, N, O, is C are perfectly overlapped, which could prove the ZIF-67 was grown on the surface of ZnO nanorods. The thickness of the ZIF-67 layer is about ~3 μm, which can provide sufficient mass loading for ES (Fig. S2).

XRD tests were further done to confirm the composition and phase structure of ZnO/ZIF-67 [Fig. 2(e)]. As shown in the XRD pattern of ZnO, there are three obvious peaks at $31.76°$, $34.42°$, and $36.25°$, corresponding to the (100), (002), and (101) planes of ZnO. The XRD pattern of the sample ZnO/ZIF-67 contains the peaks of the simulated ZIF-67. Since the ZnO/ZIF-67 were grown on the ITO glasses, we ran the XRD test of the corresponding ZIF-67 powder to get a clear picture (Fig. S3). By comparison, the XRD spectra of ZIF-67 powder contain the peaks of simulated ZIF-67. However, there are three mismatching peaks at $11.04°$, $11.85°$, and $13.87°$, corresponding to cobalt nitrate hydroxide hydrate and cobalt nitrate hydroxide, the by-products of the fast volatilization method. Thus, the successful fabrication of ZnO and ZnO/ZIF-67 was proven. Meanwhile, the strong peak of ZnO (002) could also be seen in the XRD patterns of ZnO/ZIF-67, suggesting that the main structure of the ZnO nanorod is retained after the growth of ZIF-67. The XPS tests were done to explore the valence states of the surface elements of the sample ZnO and ZnO/ZIF-67 [Figs. 2(f), S4, S5, and S6]. Corresponding peaks of the elements existing in both ZnO and ZnO/ZIF-67 were marked in the spectrum. The valence states of the surface elements were shown in the deconvolution of the XPS spectra, which is in agreement with the results of XRD. In particular, the

O 1s spectrum of the ZnO sample can be deconvoluted to two peaks located at 530.0 and 531.6 eV, corresponding to the O–H bond and the Zn–O bond, respectively. The O–H bond comes from the surface adsorbed water molecules.[35]

The bandgap energy, which describes the energy required to excite an electron from the valence band to the conduction band, is crucial in predicting the photochemical properties of a semiconductor.[36] The bandgap is obtained using the Tauc plot applied to the UV–vis data.[37] The UV–vis data of ZnO and ZIF-67 are shown in Figs. 3(a) and 3(b), and the Tauc plot is shown in the corresponding insets. The bandgaps of ZnO and ZIF-67 were calculated to be 3.09 and 1.89 eV, respectively. Moreover, in order to explore the carrier motion of the sample, the Mott–Schottky plots were done to determine the type of ZnO and ZIF-67. As shown in Figs. S7 and S8, ZnO has a positive slope in the Mott–Schottky plot, while ZIF-67 has a negative one. Thus, ZnO was identified as an n-type semiconductor and ZIF-67 as a p-type. This conclusion is consistent with previous reports. Thus, a p–n junction is formed at the ZnO/ZIF-67 interface. The energy band structures are shown in Fig. S9. When the p-type ZIF-67 and n-type ZnO are in contact, a space-charge region is formed at the interfaces of ZnO and ZIF-67 due to the diffusion of electrons and holes, creating a built-in electrical potential. Due to the internal electric field E of this p–n junction, the photogenerated electron–hole pairs are separated, and the photogenerated holes/electrons are driven toward ZIF-67 and ZnO, respectively. That is, ZnO generates electron–hole pairs under illumination, and the electrons flow through the external circuit to the counter electrode (ZIF-67/Ni foam). The more effective charge separation in the heterojunction of ZnO/ZIF-67 could enhance photo performance.

The galvanostatic charge–discharge (GCD) curves of ZnO/ZIF-67 under light (1 sun) are shown in Fig. 4(a). Photovoltage is one of the most important parameters for the performance evaluation of PV device. For the measurement of photovoltage, the sample was charged by light without applying any external current or voltage. The potential difference exhibits a rise of 0.36 V under illumination and slowly drops to 0 in the dark. As a comparison, the potential rise of ZnO is only ~0.15 V [Fig. S10(a)], suggesting the enhancement
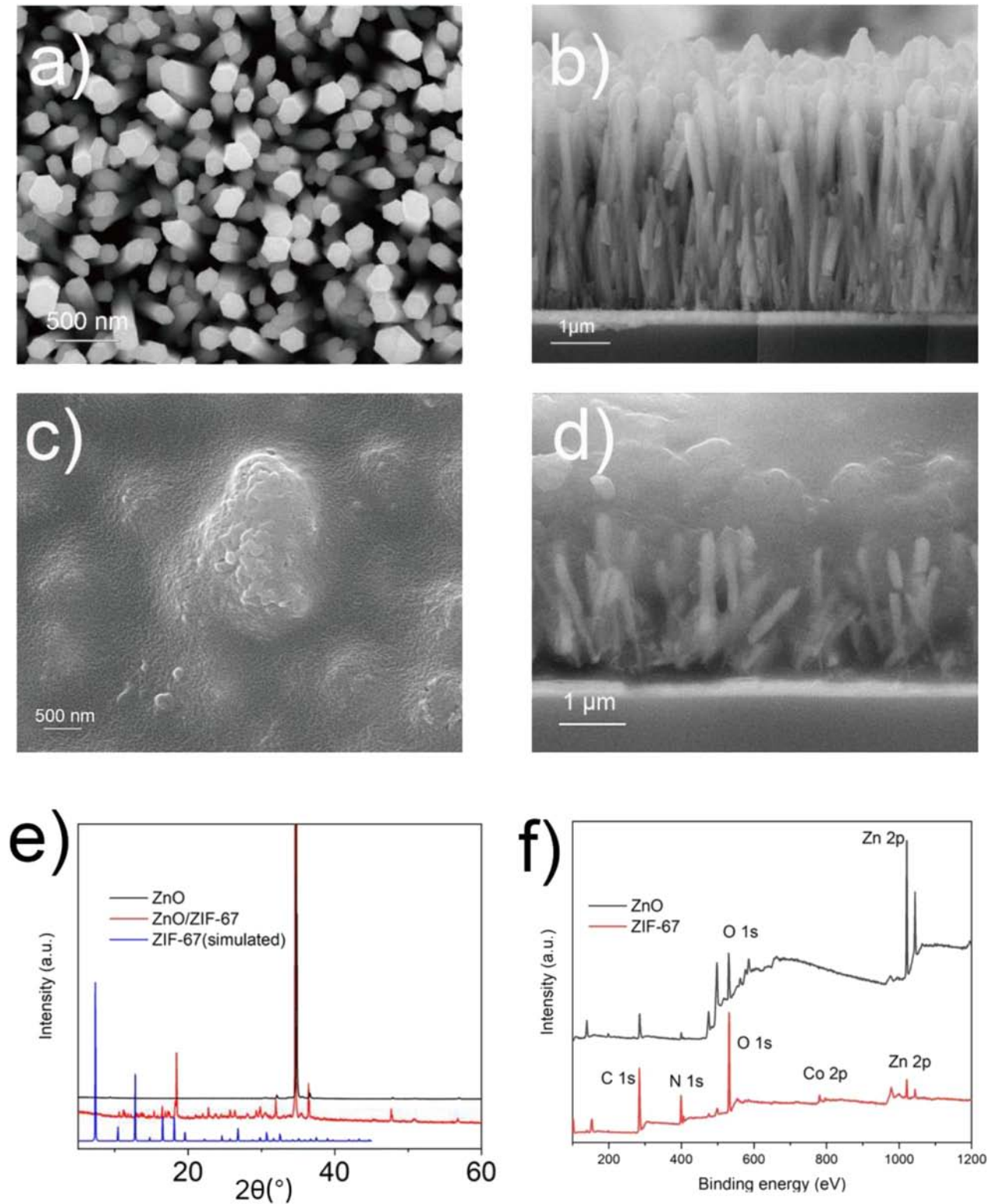
FIG. 2. (a) and (b) The surface and cross section SEM images of ZnO nanorods; (c) and (d) the surface and cross section SEM images of ZnO/ZIF-67; (e) the XRD pattern of ZnO, ZnO/ZIF-67, and ZIF-67 (simulated); and (f) the XPS spectra of ZnO and ZIF-67.
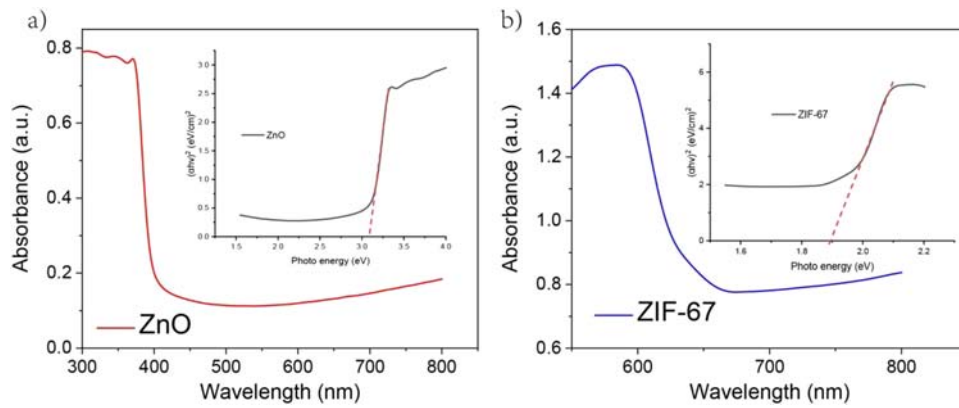
FIG. 3. UV–vis spectrum and Tauc plot (inset) of (a) ZnO and (b) ZIF-67.

from the p–n junction of the ZnO/ZIF-67 structure. The CV plots of ZnO are shown in Fig. S10(b) (2145 mF cm^{-2}). A brief comparison was listed in Table S1, containing some typical photo electrode materials such as V_2O_5, C_3N_4, and some materials based on ZnO. By comparison, the photovoltage of ZnO/ZIF-67 is among the highest

level, proving the effectiveness of the heterojunction. Moreover, the discharge current density was set as 1, 2, and 5 μA/cm^2, and the calculated specific capacity was 145.6, 144.2, and 133.5 mF/g, respectively (the mass loading is 0.52 mg/cm^2). Since the charging process was done with pure solar energy, the overall conversion
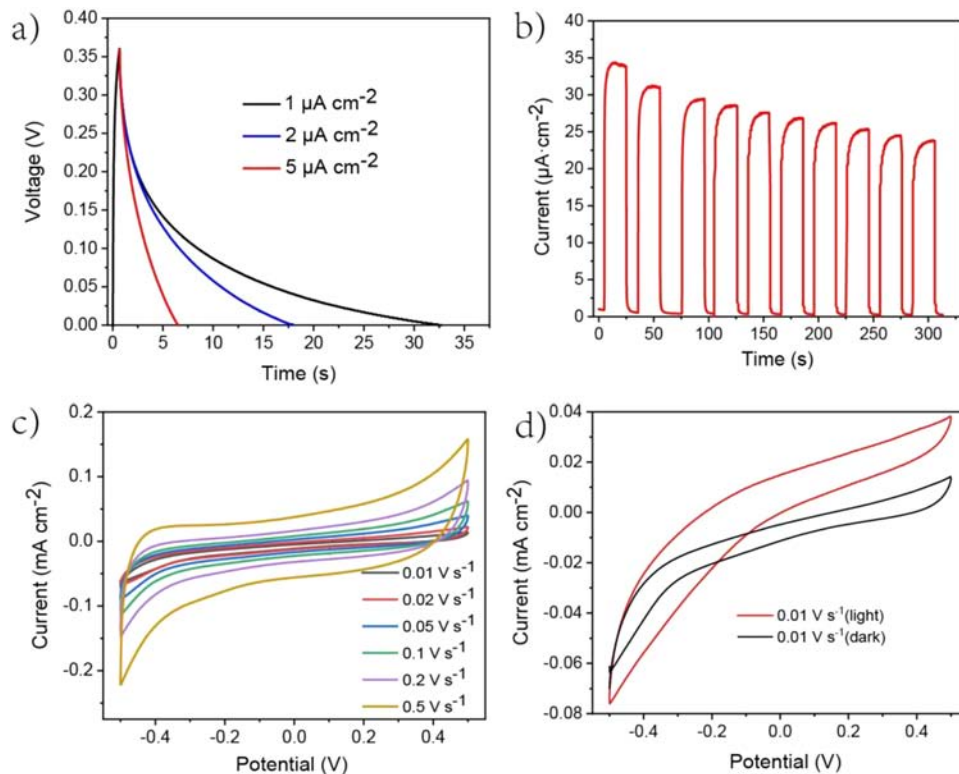

FIG. 4. (a) The galvanostatic charge–discharge curves of ZnO/ZIF-67 at different discharge current densities of 1, 2, and 5 μA cm^{-2}; (b) the absolute response current plot under dark and light at 0 V applied voltage; (c) the CV cycle plots at different scan rates from 0.01 to 0.5 V s^{-1} (dark); and (d) the CV comparison of ZnO/ZIF-67 in light and dark at the scan rate of 0.01 V s^{-1}.
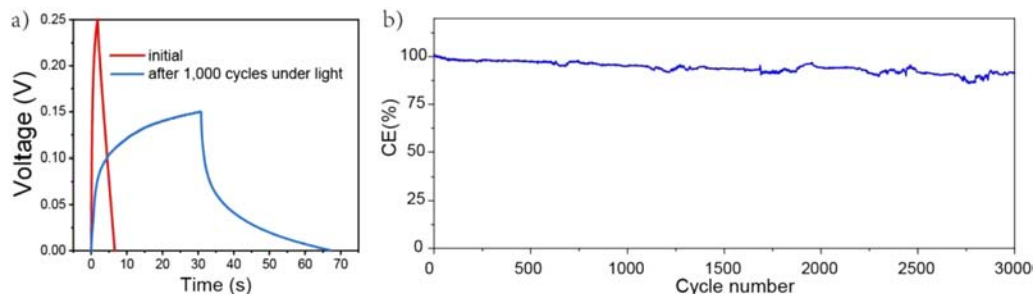
FIG. 5. The galvanostatic charge–discharge curves of the ZnO/ZIF-67 cell at the initial and 1000th cycles (light); and (b) the Coulombic efficiency during the long-term cycling in the dark.

efficiency could be calculated. The calculation details were shown in the supplementary material, and the overall efficiency was 0.49% (discharge current density at 1 μA/cm^2). During the photo charging process, the potential of ZnO/ZIF-67 went down, and the potential difference between the two electrodes rose, indicating the ZnO/ZIF-67 electrode as the photocathode. This result is consistent with the previous conclusion about the p–n hetero junction. The cyclic absolute response current is shown in Fig. 4(b). The test was done in dark and light illuminated conditions at 0 V applied voltage. The photo current dropped from ~34 to ~24 μA after ten cycles. Cyclic voltammetry (CV) of ZnO/ZIF-67 under dark conditions was carried out at different scan rates from 0.01 to 0.5 V s^{-1} [see Fig. 4(c)]. The specific capacities were calculated to be 759.0, 617.5, 443.2, 345.8, 273.9, and 206.8 mF/g, respectively. Comparatively, the CV curves under light conditions are shown in Fig. S11. It is important to point out that the light causes a capacity enhancement of ~128% at a scan rate of 0.01 V s^{-1} [Fig. 4(d)]. Electrochemical impedance spectroscopy (EIS) was also performed, and the result is represented in Fig. S12.

A cell was fabricated to explore the performance of ZnO/ZIF-67 as a practical device. Since the relative tests have been done in the two electrode test, we focus on the stability tests of the practical cell. The stability test was done under illumination and darkness for 1000 and 3000 cycles, respectively [Figs. 5(a) and 5(b)]. The photovoltage drops from ~0.24 to ~0.14 V after 1000 cycles under illumination. The Coulombic efficiency remains at 91% after 3000 cycles in the dark. The SEM images of the ZnO/ZIF-67 are shown in Figs. S13(a) and S13(b) to view the morphology after 1000 CV cycles. A certain degree of detachment can be observed over the surface layer, indicating the loss of ZIF-67 as the protective layer. As shown in the cross section images, several ZnO nanorods are exposed, and the surface becomes rough, indicating that the surface of ZnO is etched by the electrolyte. The XRD pattern of the ZnO/ZIF-67 after long-term cycles is shown in Fig. S14. Compared with the initial one, the main peaks corresponding to ZIF-67 and ZnO remain, while a few peaks of impurities appear.

IV. CONCLUSIONS

In conclusion, this work demonstrates rechargeable two-electrode PCs with a capacity of 759.0 mF/g by using the p–n heterojunction of ZnO/ZIF-67. ZnO and ZIF-67 are potential materials for PV and ES, respectively. A fast volatilization method was used to *in situ* grow ZIF-67 onto ZnO nanorods with fewer voids and interface defects. The ZIF-67 not only serves as the ES part but also forms the p–n heterojunction with ZnO. The internal electric field in the p–n heterojunction induces charge separation and generates energy band bending. As a result, the PCs show enhanced photovoltage of 0.36 V (0.15 V for single ZnO) and higher capacity in light (an increase of over 100%) upon illumination. The structural design of ZnO/ZIF-67 ensured specific capacity and enhanced photovoltage while simplifying the structure. We hope this strategy can help the development of PRDs.

SUPPLEMENTARY MATERIAL

See the supplementary material for detailed calculation and electrotest methods, TEM mapping images, SEM images, XRD spectra, XPS spectra, Mott–Schottky plots, CV plots of fabricated samples, and comparison of samples after long term stability tests.

AUTHOR DECLARATIONS

Conflict of Interest

The authors have no conflicts to disclose.

Author Contributions

Yanlong Lv: Conceptualization (equal); Data curation (lead); Formal analysis (lead); Writing – original draft (lead); Writing – review & editing (equal). **Xin Sun**: Conceptualization (equal); Data curation (lead); Formal analysis (lead); Investigation (supporting); Writing – original draft (lead); Writing – review & editing (supporting). **Changhua Mi**: Data curation (supporting); Formal analysis (supporting); Investigation (supporting); Writing – review & editing (supporting). **Jianan Gu**: Data curation (supporting); Formal analysis (supporting); Writing – review & editing (supporting). **Yanhong Wang**: Writing – review & editing (supporting). **Meicheng Li**: Conceptualization (lead); Writing – review & editing (lead).

DATA AVAILABILITY

The data that support the findings of this study are available within the article and its supplementary material.

REFERENCES

[1] T. M. L. Wigley, Nature **349**, 503–506 (1991).

[2] W.-J. Ong, L.-L. Tan, Y. H. Ng, S.-T. Yong, and S.-P. Chai, Chem. Rev. **116**, 7159–7329 (2016).

[3] M. A. Green, A. Ho-Baillie, and H. J. Snaith, Nat. Photonics **8**, 506–514 (2014).

[4] L. Yan, H. Huang, P. Cui, S. Du, Z. Lan, Y. Yang, S. Qu, X. Wang, Q. Zhang, B. Liu, X. Yue, X. Zhao, Y. Li, H. Li, J. Ji, and M. Li, Nat. Energy **8**, 1158–1167 (2023).

[5] P. Cui, D. Wei, J. Ji, H. Huang, E. Jia, S. Dou, T. Wang, W. Wang, and M. Li, Nat. Energy **4**, 150–159 (2019).

[6] M. R. Shaner, H. A. Atwater, N. S. Lewis, and E. W. McFarland, Energy Environ. Sci. **9**, 2354–2371 (2016).

[7] H. Huang, P. Cui, Y. Chen, L. Yan, X. Yue, S. Qu, X. Wang, S. Du, B. Liu, Q. Zhang, Z. Lan, Y. Yang, J. Ji, X. Zhao, Y. Li, X. Wang, X. Ding, and M. Li, Joule **6**, 2186–2202 (2022).

[8] B. Lei, G.-R. Li, P. Chen, and X.-P. Gao, Nano Energy **38**, 257–262 (2017).

[9] M. Peng, B. Dong, and D. Zou, J. Energy Chem. **27**, 611–621 (2018).

[10] P. C. Santhosh, S. Jayakumar, M. M. Mohideen, and A. V. Radhamani, Mater. Res. Bull. **174**, 112722 (2024).

[11] R. Thimmappa, B. Paswan, P. Gaikwad, M. C. Devendrachari, H. Makri Nimbegondi Kotresh, R. Rani Mohan, J. Pattayil Alias, and M. O. Thotiyl, J. Phys. Chem. C **119**, 14010–14016 (2015).

[12] Y. Hu, Y. Bai, B. Luo, S. Wang, H. Hu, P. Chen, M. Lyu, J. Shapter, A. Rowan, and L. Wang, Adv. Energy Mater. **9**, 1900872 (2019).

[13] A. Paolella, C. Faure, G. Bertoni, S. Marras, A. Guerfi, A. Darwiche, P. Hovington, B. Commarieu, Z. Wang, M. Prato, M. Colombo, S. Monaco, W. Zhu, Z. Feng, A. Vijh, C. George, G. P. Demopoulos, M. Armand, and K. Zaghib, Nat. Commun. **8**, 14643 (2017).

[14] P. Liu, H. X. Yang, X. P. Ai, G. R. Li, and X. P. Gao, Electrochem. Commun. **16**, 69–72 (2012).

[15] C. Xu, X. Zhang, L. Duan, X. Zhang, X. Li, and W. Lü, Nanoscale **12**, 530–537 (2020).

[16] H.-D. Um, K.-H. Choi, I. Hwang, S.-H. Kim, K. Seo, and S.-Y. Lee, Energy Environ. Sci. **10**, 931–940 (2017).

[17] A. Kumar, R. Hammad, M. Pahuja, R. Arenal, K. Ghosh, S. Ghosh, and T. N. Narayanan, Small **19**, 2303319 (2023).

[18] W. Yan, J. Wang, Q. Hu, J. Fu, M. K. Albolkany, T. Zhang, X. Lu, F. Ye, and B. Liu, Nano Res. **17**, 2655 (2023).

[19] T. Miyasaka and T. N. Murakami, Appl. Phys. Lett. **85**, 3932–3934 (2004).

[20] Q. Wang, H. Chen, E. McFarland, and L. Wang, Adv. Energy Mater. **5**, 1501418 (2015).

[21] V. Poojari, D. Devadiga, N. Hegde, D. N. Sangeetha, M. S. Santosh, and M. Selvakumar, J. Electrochem. Energy Convers. Storage. **17**, 031016 (2020).

[22] C.-T. Chien, P. Hiralal, D.-Y. Wang, I.-S. Huang, C.-C. Chen, C.-W. Chen, and G. A. J. Amaratunga, Small **11**, 2929–2937 (2015).

[23] J. Xu, Z. Ku, Y. Zhang, D. Chao, and H. J. Fan, Adv. Mater. Technol. **1**, 1600074 (2016).

[24] P. W. Sayyad, A. A. Farooqui, N. N. Ingle, T. Al-Gahouari, G. A. Bodkhe, M. M. Mahadik, S. M. Shirsat, and M. D. Shirsat, Chem. Phys. Lett. **776**, 138690 (2021).

[25] A. Kumar, P. Thakur, R. Sharma, A. B. Puthirath, P. M. Ajayan, and T. N. Narayanan, Small **17**, 2105029 (2021).

[26] M. Li, X. Wang, F. Li, L. Zheng, J. Xu, and J. Yu, Adv. Mater. **32**, 1907098 (2020).

[27] M. G. Nair, M. Nirmala, K. Rekha, and A. Anukaliani, Mater. Lett. **65**, 1797–1800 (2011).

[28] B. Avinash, R. C. R, N. Basavaraju, B. Abebe, T. N. Kumar, S. N. Manjula, and H. C. A. Murthy, Environ. Funct. Mater. **2**, 133–141 (2023).

[29] J. Liu, M. D. Rojas-Andrade, G. Chata, Y. Peng, G. Roseman, J.-E. Lu, G. L. Millhauser, C. Saltikov, and S. Chen, Nanoscale **10**, 158–166 (2018).

[30] R. Mimouni, B. Askri, T. Larbi, M. Amlouk, and A. Meftah, Inorg. Chem. Commun. **115**, 107889 (2020).

[31] R. Balamurugan and A. Chandra Bose, ACS Appl. Energy Mater. **7**, 974–985 (2024).

[32] D. Sheberla, J. C. Bachman, J. S. Elias, C.-J. Sun, Y. Shao-Horn, and M. Dincă, Nat. Mater. **16**, 220–224 (2017).

[33] M. Alvaro, E. Carbonell, B. Ferrer, F. Llabrés i Xamena, and H. Garcia, Chem. - Eur. J. **13**, 5106–5112 (2007).

[34] G. Jia, L. Liu, L. Zhang, D. Zhang, Y. Wang, X. Cui, and W. Zheng, Appl. Surf. Sci. **448**, 254–260 (2018).

[35] R.-H. Chang, K.-C. Yang, T.-H. Chen, L.-W. Lai, T.-H. Lee, S.-L. Yao, and D.-S. Liu, J. Nanomater. **2013**, 560542 (n.d.).

[36] P. Makuła, M. Pacia, and W. Macyk, J. Phys. Chem. Lett. **9**, 6814–6817 (2018).

[37] J. Klein, L. Kampermann, B. Mockenhaupt, M. Behrens, J. Strunk, and G. Bacher, Adv. Funct. Mater. **33**, 2304523 (2023).